Peripheral subnuclear positioning suppresses *Tcrb* recombination and segregates *Tcrb* alleles from RAG2

Elizabeth A. W. Chan[a], Grace Teng[b], Elizabeth Corbett[b], Kingshuk Roy Choudhury[c,d], Craig H. Bassing[e], David G. Schatz[b,f], and Michael S. Krangel[a,1]

Departments of [a]Immunology, [c]Radiology, and [d]Biostatistics and Bioinformatics, Duke University Medical Center, Durham, NC 27710; [b]Department of Immunobiology and [f]Howard Hughes Medical Institute, Yale University School of Medicine, New Haven, CT 06520; and [e]Department of Pathology and Laboratory Medicine, Children's Hospital of Pennsylvania, Philadelphia, PA 19104

Edited by Anjana Rao, La Jolla Institute for Allergy and Immunology, La Jolla, CA, and approved October 22, 2013 (received for review June 7, 2013)

Allelic exclusion requires that the two alleles at antigen-receptor loci attempt to recombine variable (V), diversity (D), and joining (J) gene segments [V(D)J recombination] asynchronously in nuclei of developing lymphocytes. It previously was shown that T-cell receptor β (*Tcrb*) alleles frequently and stochastically associate with the nuclear lamina and pericentromeric heterochromatin in $CD4^{-}CD8^{-}$ thymocytes. Moreover, rearranged alleles were underrepresented at these locations. Here we used 3D immunofluorescence in situ hybridization to identify recently rearranged *Tcrb* alleles based on the accumulation of the DNA-repair protein 53BP1. We found that *Tcrb* alleles recombine asynchronously in double-negative thymocytes and that V(D)J recombination is suppressed on peripheral as compared with central *Tcrb* alleles. Moreover, the recombination events that did take place at the nuclear periphery preferentially occurred on *Tcrb* alleles that were partially dissociated from the nuclear lamina. To understand better the mechanism by which V(D)J recombination is suppressed at the nuclear periphery, we evaluated the subnuclear distribution of recombination-activating gene 2 (RAG2) protein. We found that RAG2 abundance was reduced at the nuclear periphery. Moreover, RAG2 was distributed differently from RNA polymerase II and histone H3K4 trimethylation. Our data suggest that the nuclear periphery suppresses V(D)J recombination, at least in part, by segregating *Tcrb* alleles from RAG proteins.

T-cell development | thymus

Antigen receptor variable (V), diversity (D), and joining (J) gene segments are assembled by V(D)J recombination in immature T and B lymphocytes to generate diverse repertoires of T-cell receptors (TCRs) and B-cell receptors (BCRs), respectively (1). V(D)J recombination is initiated by the recombination-activating gene (RAG) 1 and 2 proteins, which bind to and induce double-strand breaks (DSBs) at recombination signal sequences that flank V, D, and J segments. V(D)J recombination at antigen-receptor loci is regulated according to cell lineage and developmental stage (2). In addition, at some loci V(D)J recombination is regulated to enforce allelic exclusion, so that a complete antigen-receptor protein is produced by only one allele (3, 4). However, the mechanisms that establish allelic exclusion are poorly understood.

Among TCR loci, only the T-cell receptor β (*Tcrb*) locus is allelically excluded (5). *Tcrb* recombination occurs in $CD4^{-}CD8^{-}$ double-negative (DN) thymocytes and is ordered, beginning with D_{β}–J_{β} rearrangement, which can occur on both alleles. Allelic exclusion then is initiated by V_{β}-to-DJ_{β} recombination, which is thought to occur asynchronously, i.e., on one allele at a time. This asynchrony allows thymocytes time to test each allele for the creation of an ORF. TCRβ proteins are sensed by their assembly with pre-Tα and CD3 chains to create a pre-TCR signaling complex; pre-TCR signals then suppress further *Tcrb* recombination and promote thymocyte proliferation and differentiation to the $CD4^{+}CD8^{+}$ double-positive (DP) stage (6).

Allelic exclusion is maintained in DP thymocytes in part by chromatin alterations, such as reduced V_{β} germ-line transcription and histone acetylation, that reduce access of RAG1/2 proteins to V_{β} gene segments (7). In addition, *Tcrb* alleles adopt a more extended, or decontracted, conformation in DP thymocytes, physically separating V_{β} and DJ_{β} segments (8). Loss of accessibility and locus decontraction both contribute to the maintenance of allelic exclusion, because V_{β} and DJ_{β} segments engineered to be accessible and proximal are capable of recombination in DP thymocytes (9, 10). However, because both *Tcrb* alleles appear to be accessible (11, 12) and contracted (8) before rearrangement in DN thymocytes, the mechanism by which the locus is biased to undergo asynchronous V_{β}-to-DJ_{β} recombination in DN thymocytes is unknown.

It has been suggested that subnuclear positioning can regulate V(D)J recombination at TCR and BCR loci. For example, association with pericentromeric heterochromatin (PCH) has been linked to the process of allelic exclusion. *Igh* loci were shown to associate with PCH monoallelically in roughly 70% of pre-B cells. Moreover, the recruited alleles were decontracted, suggesting that they had not undergone V_H rearrangement (13). *Tcrb* alleles have been shown to associate with PCH in a regulated (8) or stochastic (14) fashion in different studies. Direct analysis of rearrangement status revealed that PCH-associated *Tcrb* alleles tend not to have undergone V_{β} rearrangement (14).

The positioning of TCR and BCR alleles at the nuclear periphery also is thought to inhibit V(D)J recombination. Most *Igh* and *Igk* alleles are located at the nuclear periphery in non–B-lineage cells, whereas in pro-B cells they become more centrally located (15). This relocalization is thought to occur as a prelude

Significance

Eukaryotic genes are directed to distinct subnuclear compartments to regulate their activity. We show that different regions of the murine T-cell receptor β (*Tcrb*) locus interact independently with the nuclear lamina and that these interactions locally suppress the recombination of variable, diversity, and joining gene segments. This suppression is associated with the physical segregation of the locus from the recombinase protein, recombination-activating gene 2. Allelically excluded recombination of antigen receptor genes promotes the development of lymphocytes that each express a single antigen receptor. We propose that interaction with the nuclear lamina contributes to allelic exclusion by reducing the frequency of recombination of *Tcrb* alleles.

Author contributions: E.A.W.C. and M.S.K. designed research; E.A.W.C. performed research; G.T., E.C., C.H.B., and D.G.S. contributed new reagents/analytic tools; E.A.W.C., K.R.C., and M.S.K. analyzed data; and E.A.W.C., K.R.C., C.H.B., D.G.S., and M.S.K. wrote the paper.

The authors declare no conflict of interest.

This article is a PNAS Direct Submission.

[1]To whom correspondence should be addressed. E-mail: krang001@mc.duke.edu.

This article contains supporting information online at www.pnas.org/lookup/suppl/doi:10.1073/pnas.1310846110/-/DCSupplemental.

to expression and V(D)J recombination. *Tcrb* alleles localize stochastically to the nuclear periphery in DN thymocytes, with most nuclei having either one or two associated alleles (14). Peripheral *Tcrb* alleles were less likely than more central alleles to have undergone V_β-to-DJ_β rearrangement (14), suggesting that association with the nuclear periphery may suppress recombination and contribute to allelic exclusion. However, this analysis tracked *Tcrb* alleles that already were rearranged, so it is possible that recombination occurs freely at the nuclear periphery, with rearranged alleles subsequently relocating away from this compartment.

Here we visualized recently rearranged *Tcrb* alleles based on the assembly of foci containing DNA repair factors, and we provide evidence that *Tcrb* alleles recombine asynchronously in DN thymocyte nuclei. We found that peripheral *Tcrb* alleles are marked by repair foci less frequently than central *Tcrb* alleles. Moreover, the DNA repair foci that were detected on peripheral *Tcrb* alleles tended to occur on alleles that were partially dissociated from the nuclear lamina. To understand better why DNA repair foci are underrepresented on peripheral *Tcrb* alleles, we evaluated the location of RAG2 relative to *Tcrb* alleles and the nuclear lamina. We found that peripheral *Tcrb* alleles reside in a region of relatively low RAG2. This result suggests that the nuclear periphery helps to suppress V(D)J recombination by segregating *Tcrb* alleles from functional RAG proteins.

Results

***Tcrb* Alleles Recombine Monoallelically in DN Thymocytes.** We evaluated the frequency of recent RAG-dependent DSBs in DN thymocytes by tracking DNA-repair foci using an antibody specific for the repair protein 53BP1. 53BP1 becomes phosphorylated by ataxia-telangiectasia mutated (ATM) and is recruited to DSBs in sufficient amounts to form visible foci, indicative of ongoing or recent DNA repair (16). 53BP1 foci form within minutes of a DSB and may remain at DSB sites for several hours after their repair (17). 53BP1 also has been implicated in V(D)J recombination and class-switch recombination, functioning to protect DNA ends and to support long-range DNA interactions (18–20).

To analyze 53BP1 foci immediately ex vivo, we isolated DN thymocytes from linker for activation of T cells-negative ($Lat^{-/-}$) mice. These thymocytes are unable to signal through pre-TCR complexes and therefore cannot progress beyond the $CD44^-CD25^+$ DN3 stage of development (21). As a control, we also isolated DN thymocytes from $Rag2^{-/-}$ mice, because thymocytes are similarly blocked in development at the DN3 stage but should accumulate only random DSBs that are unrelated to V(D)J recombination. We excluded from analysis those nuclei considered to be in the process of apoptosis. Nuclei in this category (<10% of all nuclei) contained intense and broadly distributed 53BP1 staining or more than six 53BP1 foci. We chose six foci as a cutoff because that is the maximum number of *Tcrb*, *Tcrg*, and *Tcrd* alleles that potentially could undergo recombination in DN thymocytes. Among 500 $Lat^{-/-}$ nuclei analyzed, 23% contained a single 53BP1 focus, 5% contained two foci, less than 1% contained three or four foci, and none contained five or six foci (Fig. 1*A*). Similar examination of 500 $Rag2^{-/-}$ DN nuclei identified 12% with one 53BP1 focus, 0.2% with two foci, and none with three to six foci. From these results we conclude that the majority of 53BP1 foci detected in $Lat^{-/-}$ nuclei reflect DSBs resulting from V(D)J recombination. Given the overall frequency of DSBs and the rarity of nuclei with more than two DSBs, we conclude that V(D)J recombination occurs infrequently at TCR loci in DN3 thymocytes.

To identify RAG-dependent DSBs specifically at *Tcrb* alleles, we used DNA immuno-FISH to visualize 53BP1 and *Tcrb* alleles simultaneously (Fig. 1*B*). We measured the distance between the center of each 53BP1 focus and the center of the nearest *Tcrb* focus in 500 $Lat^{-/-}$ and 500 $Rag2^{-/-}$ DN thymocytes. We detected a discrete population of DSBs within 1 μm of a *Tcrb* focus in $Lat^{-/-}$ nuclei but did not detect a similar population in $Rag2^{-/-}$ nuclei. Based on this finding, we concluded that 53BP1 foci within 1 μm of a *Tcrb* allele identify *Tcrb* alleles that recently have undergone V(D)J recombination. We note that 53BP1 foci farther than 1 μm from a *Tcrb* focus were twice as frequent in $Lat^{-/-}$ as in $Rag2^{-/-}$ nuclei (118 vs. 61 foci). We presume that this increase reflects recent RAG-mediated DSBs at *Tcrg* and *Tcrd* loci in $Lat^{-/-}$ nuclei.

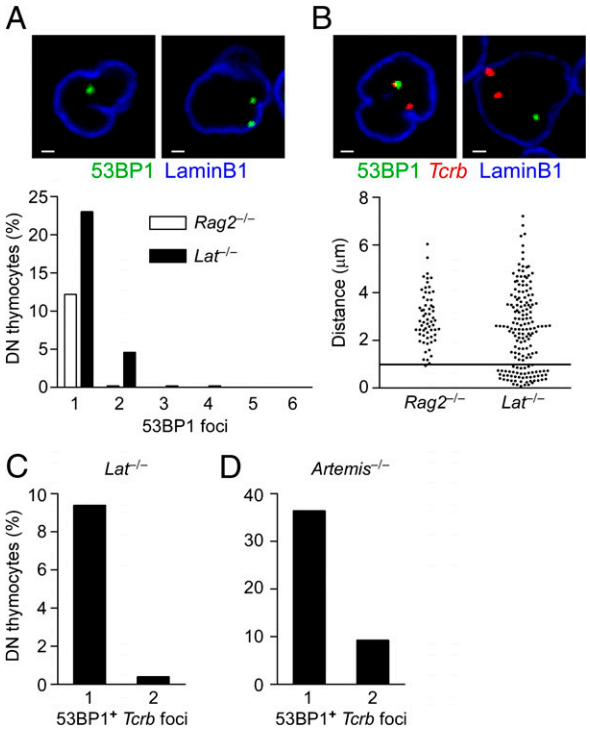

Fig. 1. *Tcrb* alleles recombine infrequently and asynchronously in $Lat^{-/-}$ DN thymocytes. (*A*) (*Upper*) Confocal immunofluorescence microscopy showing single z-slices of $Lat^{-/-}$ DN thymocyte nuclei containing one or two 53BP1 foci. (Scale bars, 1 μm.) (*Lower*) Distributions of $Rag2^{-/-}$and $Lat^{-/-}$ DN thymocyte nuclei containing one to six 53BP1 foci. (*B*) (*Upper*) Confocal immuno-FISH microscopy showing single z-slices of $Lat^{-/-}$ DN thymocyte nuclei containing 53BP1 foci at or distant from *Tcrb* foci. (Scale bars, 1 μm.) (*Lower*) Distance of 53BP1 foci from the nearest *Tcrb* allele in 500 $Rag2^{-/-}$ and 500 $Lat^{-/-}$ DN thymocyte nuclei. *Tcrb* alleles were identified using the V_β probe. The horizontal line at 1 μm separates presumed *Tcrb* 53BP1 foci from other 53BP1 foci. (*C*) Distribution of nuclei containing one or two $53BP1^+$ *Tcrb* alleles in 500 $Lat^{-/-}$ DN thymocytes. (*D*) Distribution of nuclei containing one or two $53BP1^+$ *Tcrb* alleles in 173 $Artemis^{-/-}$ DN thymocytes. Data for $Rag2^{-/-}$, $Lat^{-/-}$, and $Artemis^{-/-}$ DN thymocytes were each compiled from two independent experiments.

It has been assumed that *Tcrb* alleles may undergo synchronous D_β-to-J_β recombination followed by asynchronous V_β-to-DJ_β recombination during the initiation phase of allelic exclusion in DN thymocytes. However, direct evidence addressing either of these points has been lacking. We found that ~90% of $Lat^{-/-}$ DN thymocytes contained no $53BP1^+$ *Tcrb* alleles, 9.4% contained a single $53BP1^+$ *Tcrb* allele, and only 0.4% contained two $53BP1^+$ *Tcrb* alleles (Fig. 1*C*). A recent study demonstrated $53BP1^+$ *Tcrb* alleles in a somewhat smaller fraction (4%) of DN2/3 thymocytes of WT mice (22). In contrast to the low frequency of nuclei with two $53BP1^+$ *Tcrb* alleles in DN thymocytes of $Lat^{-/-}$ mice, we readily detected nuclei with two $53BP1^+$ *Tcrb* alleles in DN thymocytes of mice that are impaired in coding joint formation because of Artemis deficiency (Fig. 1*D*). In this case, 36.4% of DN thymocyte nuclei contained one $53BP1^+$ *Tcrb*

allele, and 9.3% contained two 53BP1$^+$ *Tcrb* alleles. The rare *Lat*$^{-/-}$ nuclei containing two 53BP1$^+$ *Tcrb* alleles could result from the simultaneous rearrangement of both alleles; however, because 53BP1 foci can remain at the site of a DSB for several hours (17, 23), they also could be explained by rearrangement events occurring hours apart. We conclude that *Tcrb* recombination occurs infrequently in *Lat*$^{-/-}$ DN thymocytes. Moreover, because the detected 53BP1 foci likely represent a mixture of D_β-to-J_β and V_β-to-DJ_β recombination events, we conclude that both steps of *Tcrb* recombination are likely to occur asynchronously on *Tcrb* alleles in DN thymocytes.

Reduced *Tcrb* Recombination at the Nuclear Periphery. The nuclear periphery is composed of inner and outer nuclear membranes, nuclear pore complexes, and the nuclear lamina (24). Approximately 40% of the chromatin in *Drosophila*, mouse, and human nuclei interact with the nuclear lamina. Regions of interacting chromatin, termed "lamin-associated domains" (LADs) (25), can span 0.1–10 Mb. LADs typically contain regions of inactive chromatin and have sharp boundaries that are demarcated by CpG islands, promoters, and CCCTC-binding factor (CTCF) sites (26–28). Although most LADs are similar across cell types, developmentally regulated genes have been shown to relocate toward or away from the nuclear lamina in a manner that generally correlates with their activation state (29–32). Additionally, when certain active genes have been forcibly repositioned to the nuclear lamina, their transcription was reduced (33–36). Therefore, the nuclear lamina is thought to represent a repressive subnuclear compartment.

Previous work showed that ~45% of DN thymocyte nuclei contain two lamin-associated *Tcrb* alleles, and an equal number contain one lamin-associated and one free allele. Within the latter subset, fully rearranged *Tcrb* alleles were substantially underrepresented at the lamina (14). To address more directly whether association with the nuclear lamina may suppress ongoing *Tcrb* recombination, we assessed the locations of recently rearranged *Tcrb* alleles in *Lat*$^{-/-}$ nuclei containing a single 53BP1$^+$ *Tcrb* allele and a single *Tcrb* allele in contact with the nuclear lamina. We scored contact when two adjacent pixels were positive for both laminB1 staining and *Tcrb* hybridization. When association with the lamina was assessed using a probe hybridizing with the V_β end of the *Tcrb* locus (Fig. 2*A*), 53BP1$^+$ foci were not significantly underrepresented on WT *Tcrb* alleles in *Lat*$^{-/-}$ thymocytes (Fig. 2*B*).

The D_β-to-J_β and V_β-to-DJ_β steps of *Tcrb* recombination could be differentially affected by V_β-end contact with the lamina. Therefore, a specific effect on one step of recombination could have been masked in the above experiment. To distinguish 53BP1 foci arising from the two steps of recombination, we used gene-targeted mice carrying modified *Tcrb* alleles that can undergo only D_β-to-J_β or only V_β-to-DJ_β recombination events (Fig. 2*A*). The M4 *Tcrb* allele has a mutation in the 5′ $D_\beta1$ RSS and lacks the $D_\beta2J_\beta2$ cluster, and thus it can undergo only D_β-to-J_β recombination (37). The DJβ allele has a pre-rearranged $DJ_\beta1$ gene segment and lacks the $D_\beta2J_\beta2$ cluster and thus can undergo only V_β-to-$DJ_\beta1$ recombination (38). The ω allele serves as a useful control because it lacks the $D_\beta2J_\beta2$ cluster but has an unmanipulated $D_\beta1J_\beta1$ cluster and thus can undergo both D_β-to-$J_\beta1$ and V_β-to-$DJ_\beta1$ recombination (37). All modified alleles were crossed onto a *Lat*$^{-/-}$ background to allow the direct harvest and analysis of DN thymocytes immediately ex vivo. Consistent with the loss of half of the D_β and J_β segments, the frequency of 53BP1$^+$ ω *Tcrb* alleles was roughly half that of WT alleles (Fig. 2*A*). The frequencies of 53BP1$^+$ M4 and DJβ alleles were only slightly lower (Fig. 2*A*). We note that 53BP1 foci reflecting V_β-to-$DJ_\beta1$ recombination may be more frequent in DJβ/DJβ *Lat*$^{-/-}$ than in ω/ω *Lat*$^{-/-}$ nuclei because V_β-to-DJ_β recombination was found to occur more efficiently on alleles that already have undergone D_β-J_β recombination (38).

Similar to the results obtained with *Lat*$^{-/-}$ thymocytes, we found no evidence that 53BP1 foci were underrepresented on *Tcrb* alleles anchored to the nuclear lamina by the V_β end in either ω/ω *Lat*$^{-/-}$ or M4/M4 *Lat*$^{-/-}$ thymocytes (Fig. 2*B*). However, DJβ/DJβ *Lat*$^{-/-}$ thymocytes behaved differently, because only 26% of 53BP1 foci occurred on *Tcrb* alleles in contact with the nuclear lamina, and 74% occurred on free alleles. This result implies that V_β-end association with the nuclear lamina suppresses the V_β-to-DJ_β but not the D_β-to-J_β step of *Tcrb* recombination.

Given the selective impact of V_β-end association on V_β-to-DJ_β recombination, we hypothesized that recombination could be differentially influenced depending on the nature of *Tcrb* locus contact with the nuclear lamina. Therefore, we also scored *Tcrb*–lamin colocalization using a probe that detects the C_β end of the *Tcrb* locus (Fig. 2 *A* and *C*). We observed substantially reduced frequencies of 53BP1$^+$ foci on C_β end-associated *Tcrb* alleles in *Lat*$^{-/-}$, M4/M4 *Lat*$^{-/-}$, and DJβ/DJβ *Lat*$^{-/-}$ thymocytes (Fig. 2*C*). We also observed a similar trend in ω/ω *Lat*$^{-/-}$ thymocytes, al-

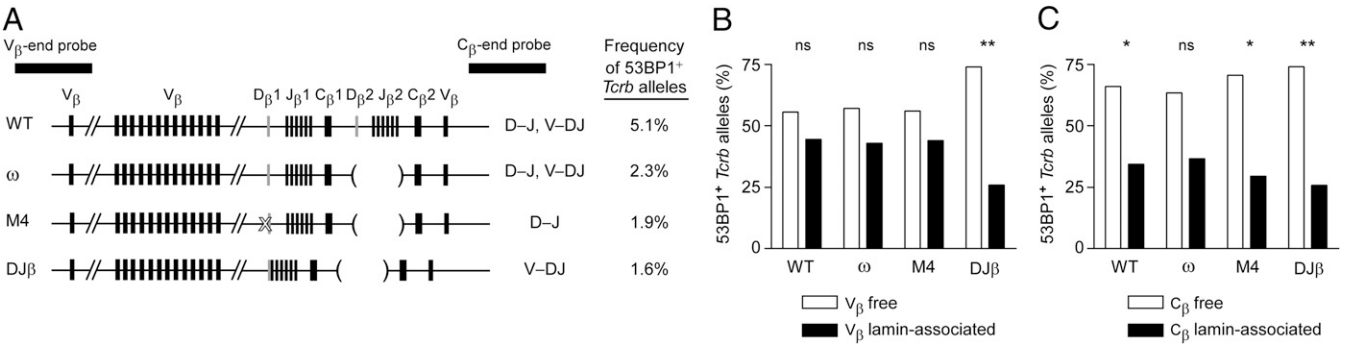

Fig. 2. *Tcrb* recombination is suppressed at the nuclear periphery. (*A*) Diagram of modified *Tcrb* alleles and location of V_β-end and C_β-end DNA probes. WT and ω alleles can undergo D_β-to-J_β and V_β-to-DJ_β recombination, whereas M4 alleles can undergo only D_β-to-J_β and DJβ alleles can undergo only V_β-to-DJ_β recombination. Frequencies of 53BP1 foci were calculated from 500 WT, 1,100 ω, 1,525 M4, and 394 DJβ nuclei on two to four slides per genotype. (*B*) Frequencies of lamin-associated and free 53BP1$^+$ *Tcrb* alleles in *Lat*$^{-/-}$ DN thymocyte nuclei having a single 53BP1$^+$ *Tcrb* allele and monoallelic *Tcrb* association with the nuclear lamina. *Tcrb* association with the lamina was scored using a V_β-end probe on 63 WT, 56 ω, 61 M4, and 54 DJβ nuclei (five to eight slides per genotype). (*C*) *Tcrb* association with the lamina was scored using a C_β-end probe on 70 WT, 52 ω, 51 M4, and 58 DJβ nuclei (four to eight slides per genotype). Fisher's exact two-tailed contingency tables were used to compare frequencies of lamin-associated 53BP1$^+$ *Tcrb* alleles to the frequency of total lamin-associated *Tcrb* alleles (50%). $^*P < 0.05$; $^{**}P < 0.01$; ns, not significant.

though the result fell short of statistical significance (Fig. 2*C*). These results imply that C_β-end association with the nuclear lamina suppresses both the D_β-to-J_β and V_β-to-DJ_β steps of *Tcrb* recombination. We conclude that the V_β and C_β ends of the locus may associate with the nuclear lamina independently. Tethering by the V_β end selectively inhibits V_β-to-DJ_β recombination because the distant D_β and J_β segments may remain free of the nuclear lamina and available for recombination. In contrast, tethering by the C_β end inhibits both D_β-to-J_β and V_β-to-DJ_β recombination because only the distant V_β segments may remain free of the lamina on these alleles.

Distinct Conformations of *Tcrb* Alleles at the Nuclear Lamina. Independent interactions of the V_β and C_β ends suggest that lamin-associated *Tcrb* alleles may adopt distinct conformations relative to the nuclear lamina that may be suppressive or permissive for recombination. To assess this possibility more directly, we evaluated the orientation of lamin-associated 53BP1$^+$ and total *Tcrb* alleles by deconvolving 3D images and measuring the distances between the nearest point on the inner surface of the nuclear lamina and the centers of *Tcrb* and 53BP1 foci.

We first analyzed the conformations of peripheral *Tcrb* alleles by comparing the locations of the V_β and C_β ends of individual *Tcrb* alleles relative to the nuclear lamina in *Lat*$^{-/-}$ thymocytes (Fig. 3*A*, *Left*). We then calculated the extent to which one end of the *Tcrb* locus was more embedded in the lamina or more nucleoplasmic than the other end (Fig. 3*B*). Alleles anchored to the lamina via the V_β end displayed a spectrum of conformations. On most alleles the C_β end was displaced less than 100 nm relative to the V_β end (Fig. 3*C*, *Left*). However, on some alleles the C_β end was substantially more nucleoplasmic than the V_β end. Similar conclusions were reached for V_β-end displacement when the C_β end was positioned at the lamina (Fig. 3*D*, *Left*). These data suggest that the entire lengths of most peripheral *Tcrb* loci interact with the lamina, whereas on some alleles one end may be free of the lamina. These observations held true for the modified *Tcrb* alleles as well, showing that none of the modifications substantially influence the conformation of the *Tcrb* locus relative to the lamina.

We then analyzed the displacement of 53BP1 foci relative to the lamin-associated V_β end of the *Tcrb* locus (Fig. 3*A*, *Center* and Fig. 3*C*, *Right*). 53BP1 foci almost always were farther from the lamina than the lamin-associated V_β end, being on average 150–230 nm more nucleoplasmic in the different genotypes. This observation suggests that, although V(D)J recombination is suppressed by the nuclear lamina, V_β-to-DJ_β and D_β-to-J_β recombination may occur on *Tcrb* alleles that have partially dissociated on the C_β end.

Similarly, 53BP1 foci were farther from the lamina than the lamin-associated C_β end of the *Tcrb* locus, being on average 87–126 nm more nucleoplasmic in the different genotypes (Fig. 3*A*, *Right* and Fig. 3*D*, *Right*). That 53BP1 foci tended to be less well separated from the C_β end than from the V_β end makes sense, because the C_β-end probe is centered ~140 kb downstream of the D_β and J_β segments, whereas the V_β-end probe is centered ~325 kb upstream of the center of the V_β array (Fig. 2*A*). We conclude that the full lengths of most *Tcrb* alleles are in contact with the nuclear lamina but that V(D)J recombination occurs preferentially on the subset of peripheral alleles that have partially dissociated from the lamina.

RAG2 Levels Are Reduced at the Nuclear Periphery. Contact of the *Tcrb* locus with the nuclear lamina could function to suppress V(D)J recombination by inhibiting transcription and accessibility of *Tcrb* alleles. However, prior work indicated that V_β segments are transcribed biallelically in all DN thymocytes (12). Another possibility is that peripheral *Tcrb* loci might be inhibited from undergoing V(D)J recombination because of their segregation from

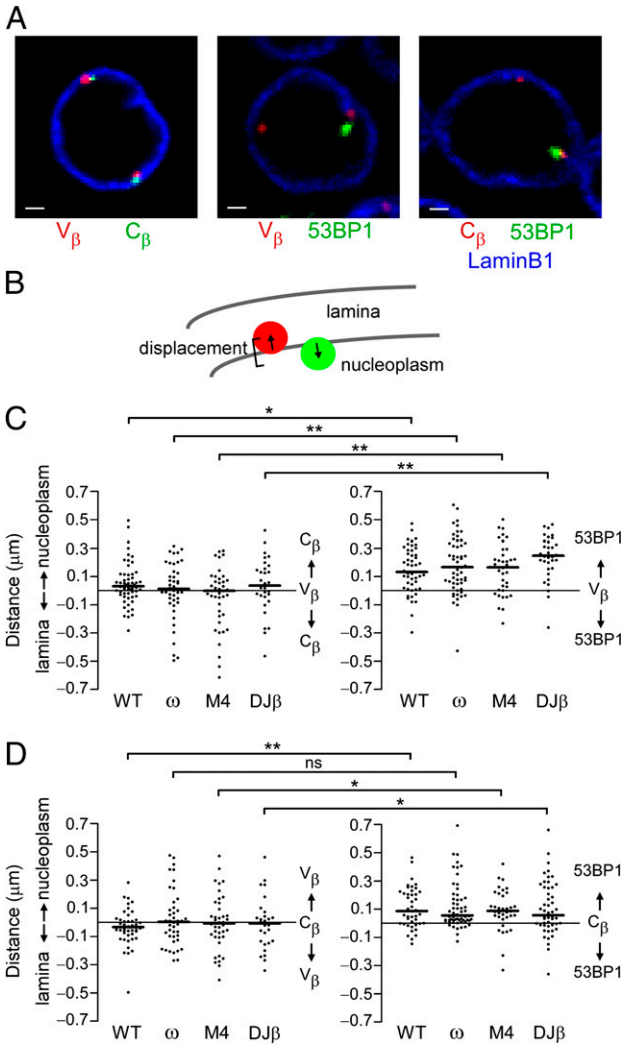

Fig. 3. Orientation of lamin-associated *Tcrb* alleles. (*A*) Confocal immuno-FISH microscopy showing single z-slices of *Lat*$^{-/-}$ DN thymocyte nuclei containing lamin-associated *Tcrb* alleles. *Tcrb* alleles were characterized using the V_β-end probe, the C_β-end probe, and anti-53BP1. (Scale bars, 1 μm.) (*B*) Schematic of methodology used to determine the displacement of one focus (V_β, C_β, or 53BP1) from the defined lamin-associated focus (V_β or C_β). (*C*) (*Left*) V_β-end and C_β-end DNA probes were used to determine the relative location of the C_β end when the V_β end is positioned at the lamina. Positive values indicate that the C_β end is farther from the lamina than the V_β end; negative values indicate that the C_β end is embedded in the lamina more deeply than the V_β end. (*Right*) A V_β-end probe and anti-53BP1were used to determine the relative location of 53BP1 foci when the V_β end is positioned at the lamina. Positive values indicate that 53BP1 is farther from the lamina than the V_β end; negative values indicate that 53BP1 is more deeply embedded in the lamina than the V_β end. (*D*) (*Left*) V_β-end and C_β-end DNA probes were used to determine the relative location of the V_β end when C_β end is positioned at the lamina. Positive values indicate that the V_β end is farther from the lamina than the C_β end; negative values indicate that the V_β end is more deeply embedded in the lamina than the C_β end. (*Right*) A C_β-end probe and anti-53BP1 were used to determine the relative location of 53BP1 foci when the C_β end is positioned at the lamina. Positive values indicate that 53BP1 is farther from the lamina than the C_β end; negative values indicate that 53BP1 is more deeply embedded in the lamina than the C_β end. All alleles were analyzed on a *Lat*$^{-/-}$ background. Each V_β–C_β analysis was conducted on one slide per genotype. V_β–53BP1 and C_β–53BP1 analyses were conducted on two to five slides per genotype. Heavy black lines denote median displacement. $^*P < 0.05$; $^{**}P < 0.01$; ns, not significant, by unpaired, two-tailed *t* tests.

RAG proteins. In this regard, a recent publication demonstrated that the histone H3 lysine 4 trimethylation (H3K4me3) modification is sequestered to the nuclear interior (39). Because RAG2

contains a plant homeodomain (PHD) finger that interacts with H3K4me3 (40-42), functional RAG proteins may be similarly sequestered. Therefore we investigated the subnuclear distribution of RAG2 relative to the nuclear lamina.

An anti-RAG2 monoclonal antibody (43) detected punctate staining of variable intensity in about 70% of $Lat^{-/-}$ nuclei but not in control $Rag2^{-/-}$ nuclei (Fig. 4*A*). We also costained with anti-Ki67, because this protein marks cycling cells (44), and RAG2 is degraded in a cell-cycle–dependent fashion (45). As expected, RAG2 staining was generally low in the $Ki67^{+}$ subset (~15%) of $Lat^{-/-}$ nuclei but was readily detected in most $Ki67^{low}$ nondividing nuclei (Fig. 4*A*). Within $RAG2^{+}$ nuclei, RAG2 staining was excluded from areas of heterochromatin, defined by concentrated DAPI staining (Fig. 4*B*). To provide further evidence for staining specificity, we examined additional populations of T and B cells. As expected from the known expression characteristics of RAG2 protein, staining with anti-RAG2 was detected in DP thymocytes but not in more mature $CD4^{+}CD8^{-}$ thymocytes (Fig. S1*A*). Staining also was observed in pro-B cells but not in mature peripheral B cells (Fig. S1*B*). The punctate staining distributions in DP thymocyte and pro–B-cell nuclei were similar to those observed in DN thymocyte nuclei.

To evaluate the RAG2 distribution relative to the nuclear periphery, we deconvolved 3D images and obtained fluorescence intensity traces across the nuclear diameter of individual thymocytes. These traces revealed peaks of RAG2 staining between laminB1 peaks in $Lat^{-/-}$ but not $Rag2^{-/-}$ control nuclei (Fig. 4*C*). We then summed fluorescence intensity plots from 40 nuclear edges per experiment to obtain average distributions of RAG2 in $Lat^{-/-}$ and $Rag2^{-/-}$ nuclei relative to peak lamin intensity (Fig. 4*D*). These results revealed that RAG2 staining does not reach maximum intensity until nearly 1 μm from peak lamin staining, suggesting that RAG2 is excluded from the nuclear periphery.

Segregation of Peripheral *Tcrb* Alleles from RAG2. To understand the distribution of *Tcrb* alleles relative to the nuclear periphery and RAG2, we obtained traces measuring the shortest distance between peak intensities of *Tcrb* foci and the nuclear lamina. *Tcrb* alleles, on average, distributed very close to the nuclear lamina (Fig. 5*A*). In fact, they were as close to the lamina as the most peripheral DNA, defined by DAPI staining. In this position, most *Tcrb* alleles were segregated from the highest concentrations of RAG2. In contrast, *Tcra*/*Tcrd* alleles, which are not allelically excluded, were distributed more centrally in the nucleus in an environment characterized by high levels of RAG2 (Fig. 5*A*).

To analyze further the spatial relationships between *Tcrb* alleles and RAG2, we simultaneously visualized *Tcrb* alleles and RAG2 protein in individual DN thymocyte nuclei (Fig. 5*B*). The great majority of *Tcrb* alleles embedded within the nuclear lamina did not colocalize with RAG2 foci (Fig. 5*B*, *i* and Fig. 5*C*, right bar). Moreover, *Tcrb* alleles in contact with the nuclear lamina (Fig. 5*B*, *ii–v* and Fig. 5*C*, center bar) colocalized with RAG2 foci less frequently than did free *Tcrb* alleles (Fig. 5*B*, *vi–viii* and Fig. 5*C*, left bar). Taken together, these data suggest that positioning at the nuclear periphery reduces the frequency with which *Tcrb* alleles interact with RAG2.

The Subnuclear Distribution of RAG2 Is Distinct from That of RNA Polymerase II and H3K4me3. The experiments described above raise the question of what determines the subnuclear distribution of RAG2 proteins. We characterized the subnuclear distributions of H3K4me3 and RNA polymerase II (PolII) in $Lat^{-/-}$ DN thymocyte nuclei by staining with specific antibodies and comparing fluorescence intensity plots with those for the nuclear lamina, RAG2, and DAPI staining (Fig. 6*A*). Antibodies used for H3K4me3 and PolII staining were judged to be specific based on blocking with the respective immunogenic peptides (Fig. 6 *B* and

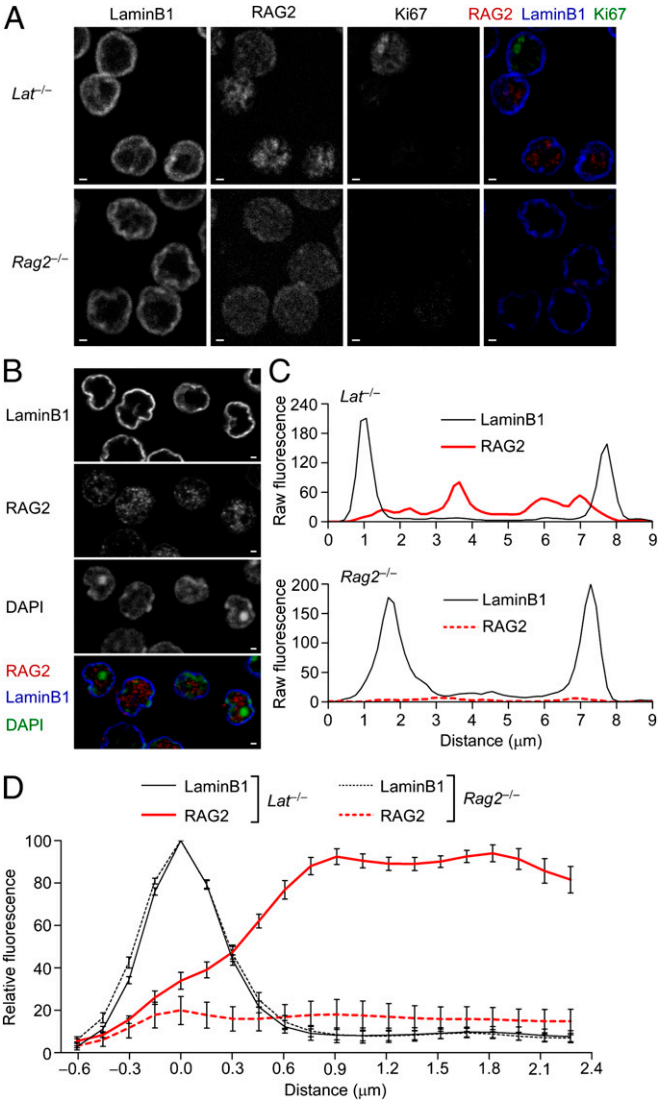

Fig. 4. RAG2 protein is reduced at the nuclear periphery. (*A*) Confocal immunofluorescence microscopy showing subnuclear localization of RAG2 relative to laminB1 in nuclei of $Lat^{-/-}$ and $Rag2^{-/-}$ DN thymocytes. Ki67 staining was used to identify cycling cells. Raw laminB1, RAG2, and Ki67 images were background-subtracted and merged (*Right*). (Scale bars, 1 μm.) (*B*) Localization of laminB1, RAG2, and DAPI in nuclei of $Lat^{-/-}$ DN thymocytes. Raw laminB1, RAG2, and DAPI images were background-subtracted and merged (*Bottom*). (Scale bars, 1 μm.) (*C*) Sample RAG2 and laminB1 fluorescence intensity plots across the diameter of a single z-slice of a $Lat^{-/-}$ and a $Rag2^{-/-}$ DN thymocyte nucleus. Slides were costained with anti-RAG2 and anti-laminB1. Slides containing $Lat^{-/-}$ and $Rag2^{-/-}$ nuclei were simultaneously stained and were imaged under identical conditions to allow evaluation of relative fluorescence intensities. (*D*) Normalized RAG2 and laminB1 fluorescence intensity distributions across $Lat^{-/-}$ and $Rag2^{-/-}$ DN thymocyte nuclei. Traces across individual nuclei were aligned at the point of peak laminB1 staining (x = 0). Data were collected and summed for 40 nuclear edges per experiment. For $Lat^{-/-}$ nuclei, maximal laminB1 and RAG2 staining in each experiment was normalized to 100. For $Rag2^{-/-}$ nuclei, laminB1 staining was normalized similarly, but RAG2 staining was normalized to the maximum fluorescence intensity in the corresponding $Lat^{-/-}$ experiment. Each trace represents the mean ± SEM of five independent experiments.

E). Neither H3K4me3 nor PolII fluorescence intensity extended as close to the nuclear lamina as total DNA, in agreement with the idea that the nuclear periphery generally is transcriptionally repressive. However, H3K4me3 and PolII staining appeared to peak slightly closer to the nuclear lamina than RAG2 staining,

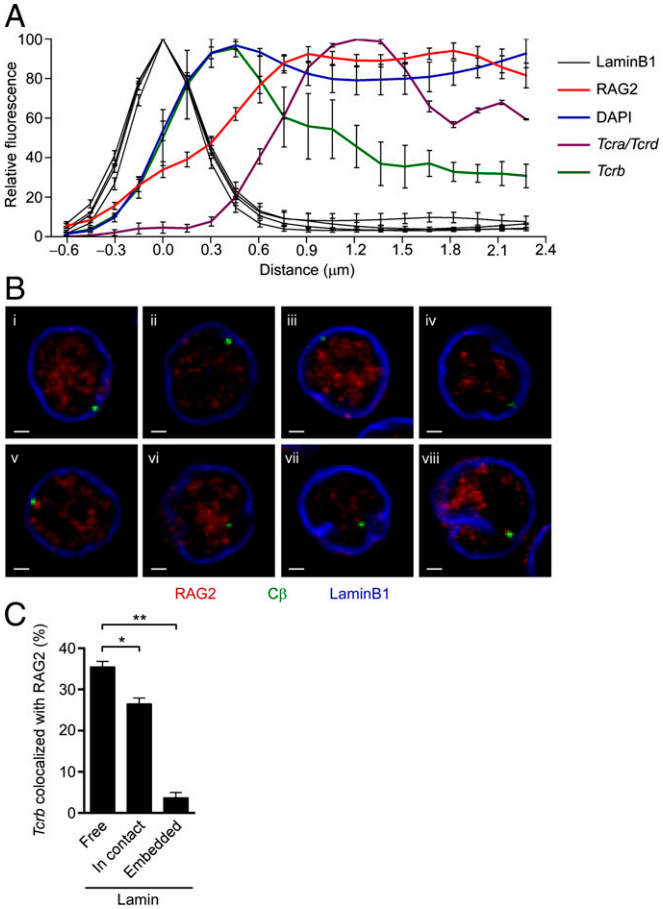

Fig. 5. Peripheral *Tcrb* alleles are physically separated from RAG2 proteins. (*A*) Normalized *Tcrb*, *Tcra/Tcrd*, DAPI, RAG2, and laminB1 fluorescence intensity distributions across $Lat^{-/-}$ DN thymocyte nuclei. The RAG2 fluorescence intensity plot and the corresponding laminB1 fluorescence intensity plot are from Fig. 4*D*. *Tcrb*, *Tcra/Tcrd*, and DAPI stains were conducted independently, each with a corresponding laminB1 stain. Traces across individual nuclei were aligned at the point of peak laminB1 staining (x = 0). DAPI staining was collected and summed for 40 nuclear edges per experiment and *Tcrb* and *Tcra/Tcrd* for 50 alleles per experiment, with the point of maximal staining normalized to 100 in each experiment. Data for DAPI are presented as mean ± SEM of three independent experiments; data for *Tcrb* and *Tcra/Tcrd* are presented as mean ± SEM of two independent experiments. (*B*) Confocal immuno-FISH microscopy showing the relative locations of *Tcrb* foci, RAG2, and laminB1 in single z-slice images of $Lat^{-/-}$ DN thymocyte nuclei. *Tcrb* alleles were identified by hybridization with the C_β-end probe. (Scale bars, 1 μm.) (*C*) Frequencies with which *Tcrb* alleles that are free of, in contact with, or embedded in the nuclear lamina colocalize with RAG2. *Tcrb* foci were considered to be lamin-free if fewer than two adjacent pixels colocalized with lamin signal. Foci were considered to be lamin-embedded if ≥90% of all *Tcrb* pixels colocalized with lamin signal; they were considered to be in contact with the lamina if more than two adjacent pixels but <90% of all pixels colocalized with lamin signal. Data were collected from 289 lamin-free, 318 lamin-contacting, and 99 lamin-embedded *Tcrb* alleles in four independent experiments. $*P < 0.05$ and $**P < 0.01$, by unpaired, two-tailed *t* tests.

suggesting that the RAG2 distribution may not be defined by either factor.

To evaluate better the subnuclear relationship between RAG2 and PolII, we simultaneously visualized both proteins in individual thymocyte nuclei (Fig. 6*B*). The distributions of the two proteins overlapped only partially, with minimal correlation between the two fluorescence intensity signals in individual thymocyte nuclei (Fig. 6*C*, *Left*) and as averaged over many nuclei in several independent experiments (Fig. 6*D*). Hence RAG2 protein does not localize primarily to transcription factories.

Technical limitations prevented us from directly comparing the RAG2 distribution with that of H3K4me3. However, we were able to covisualize H3K4me3 and PolII (Fig. 6*E*). We observed substantially overlapping and highly correlated distributions (Fig. 6*C*, *Right*, and *D*), consistent with the localization of H3K4me3 near the promoters of actively transcribed genes (46). Thus, although RAG2 has a PHD domain that binds H3K4me3 (40, 41), and chromatin-bound RAG2 colocalizes with H3K4me3 genome wide (47), we infer that the distribution of total RAG2 protein in DN thymocyte nuclei is unlikely to correspond well to the distribution of H3K4me3.

To address the role of H3K4me3 in determining the subnuclear distribution of RAG2 protein independently, we analyzed the RAG2 distribution in DN thymocytes of mice expressing a truncated RAG2 protein that lacks its C-terminal region, including the PHD domain (48). Comparison of $Rag^{\Delta/\Delta}$ $Lat^{-/-}$ and $Lat^{-/-}$ DN thymocytes revealed indistinguishable distributions of RAG2 protein relative to the nuclear lamina in the two cell populations (Fig. 7). This result indicates that binding to H3K4me3 does not limit RAG2 protein from the nuclear periphery and reinforces the notion that binding to H3K4me3 does not dictate the subnuclear distribution of total RAG2 protein.

***Tcrb* Alleles Predominantly Colocalize with PolII.** Because the nuclear lamina is thought to be repressive for transcription, the inhibition of V(D)J recombination on peripheral *Tcrb* alleles could reflect, in part, segregation from RNA PolII and reduced transcription and accessibility to RAG proteins. To address this point, we simultaneously visualized *Tcrb* alleles and PolII in DN thymocyte nuclei (Fig. 8*A*). Almost all *Tcrb* alleles colocalized with PolII signal, regardless of their peripheral localization (Fig. 8 *A* and *B*). Notably, *Tcrb* alleles almost always were positioned at the edge of regions of PolII staining, and we often observed finger-like projections of PolII extending to *Tcrb* alleles at the nuclear lamina (Fig. 8*A*, *i* and *vii*). Moreover, in most nuclei, both *Tcrb* alleles were in contact with PolII (Fig. 8*A*, *i–iv* and *vi*). Thus, our results are consistent with previous work demonstrating that V_β gene segments are transcribed biallelically in DN thymocyte nuclei (12). We conclude that the peripheral location of many *Tcrb* alleles may limit recombination primarily by impacting the supply of RAG2 to accessible *Tcrb* alleles.

Discussion

Previously we showed that *Tcrb* alleles stochastically localize to the nuclear periphery and that peripheral *Tcrb* alleles are less likely to have undergone V_β-to-DJ_β recombination. Here we found a reduction of $53BP1^+$ *Tcrb* alleles at the nuclear periphery, offering strong support for the notion that ongoing *Tcrb* recombination is suppressed by interaction of *Tcrb* alleles with the nuclear lamina. We analyzed the conformation of peripheral $53BP1^+$ *Tcrb* alleles relative to the lamina and found that those 53BP1 foci that do occur on peripheral *Tcrb* alleles tend to be farther from the nuclear lamina than the lamin-associated end of the *Tcrb* locus. This observation suggests that tight association with the lamina is strongly suppressive for V(D)J recombination and that recombination events are favorable only when a substantial portion of the locus has dissociated from the lamina. Notably, we found that the abundance of RAG2 protein was reduced in the vicinity of the nuclear lamina, implying that segregation from RAG2 contributes to the peripheral suppression mechanism. Given the high frequency with which *Tcrb* alleles associate with the nuclear lamina, we propose that this association can serve an important function by limiting biallelic *Tcrb* recombination in DN thymocytes, thereby setting the stage for allelic exclusion.

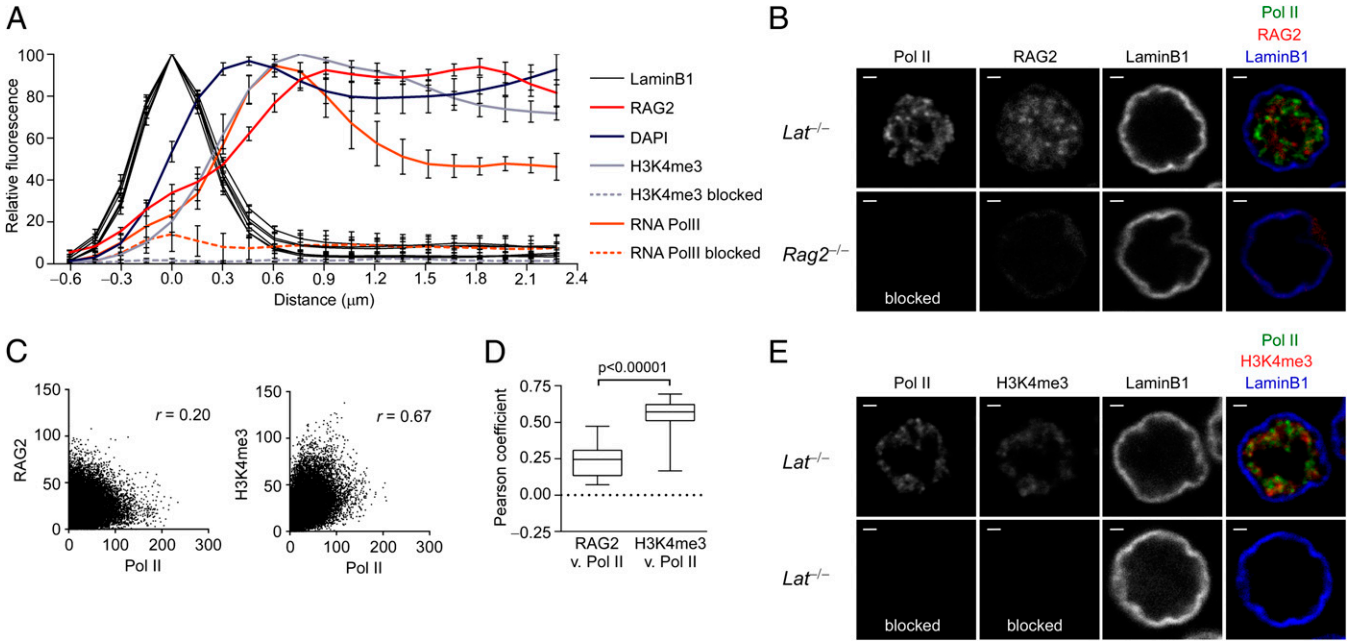

Fig. 6. RAG2 protein distribution is distinct from that of PolII and H3K4me3. (*A*) Normalized distributions of PolII, peptide immunogen-blocked PolII, H3K4me3, peptide immunogen-blocked H3K4me3, DAPI, RAG2, and laminB1 fluorescence intensity across *Lat*$^{-/-}$ DN thymocyte nuclei. The RAG2 and DAPI fluorescence-intensity plots and their corresponding laminB1 fluorescenc-intensity plots are from Figs. 4*D* and 5*A*, respectively. Slides for H3K4me3 and blocked H3K4me3 were stained simultaneously and imaged under identical conditions to allow evaluation of relative fluorescence intensity. Slides for PolII and blocked PolII were treated similarly. Staining was collected and summed for 40 nuclear edges per experiment. Maximal H3K4me3 and PolII staining was normalized to 100 in each experiment. In each case, control (blocked) staining was normalized to the maximum fluorescence intensity in the corresponding experimental (unblocked) staining. Corresponding laminB1 traces are presented for all experiments. Data for H3K4me3, blocked H3K4me3, PolII, and blocked PolII each represent the mean ± SEM of three independent experiments. (*B*) Confocal immunofluorescence microscopy showing subnuclear localization of PolII, RAG2, and laminB1 in nuclei of *Lat*$^{-/-}$ and *Rag2*$^{-/-}$ DN thymocytes. Raw PolII, RAG2, and laminB1 images were background-subtracted and merged (right-most panels). (Scale bars, 1 μm.) (*C*) Correlation analysis of RAG2 and PolII fluorescence intensity (*Left*) and of H3K4me3 and PolII fluorescence intensity (*Right*) in all voxels of single *Lat*$^{-/-}$ DN thymocyte nuclei. *r*, Pearson correlation coefficient. (*D*) Box-and-whisker plots of Pearson correlation coefficients for distributions of RAG2 vs. PolII (total of 43 nuclei in two independent experiments) and H3K4me3 vs. PolII (total of 61 nuclei in two independent experiments). Statistical significance was evaluated by unpaired *t* test. (*E*) Confocal immunofluorescence microscopy showing subnuclear localization of PolII, H3K4me3, and laminB1 in nuclei of *Lat*$^{-/-}$ DN thymocytes. Raw PolII, RAG2, and laminB1 images were background-subtracted and merged (right-most panels). (Scale bars, 1 μm.)

Our conclusions rest on the assumption that repair of RAG-induced DSBs occurs in the same location in which they were generated. DSB repair in yeast has been shown to involve movement and clustering of DNA repair foci (49). Studies of DSB repair following radiation-induced damage in mammalian nuclei have documented mobility and clustering of repair foci, as in yeast (50), or minimal mobility that is no greater than that of undamaged chromatin (51, 52). Notably, positional stability also was documented for single enzymatically induced DSBs (53, 54). This result also is consistent with studies indicating that chromosomal translocations tend to occur between loci that already are in spatial proximity at the time of DNA damage (53-56). Thus, we think it likely that the *Tcrb*-proximal 53BP1 foci we observe mark the subnuclear sites of *Tcrb* recombination events.

RAG-induced DSBs activate the ATM kinase, which aids in efficient DSB repair (57). ATM recently was shown to help enforce allelic exclusion at *Igk* loci by downregulating *Rag1* and *Rag2* transcription in response to a RAG-induced DSB (58). Transient suppression of recombination by this mechanism could guarantee asynchronous recombination by preventing recombination on the second allele while the first allele is being repaired and tested for functionality. Should such a mechanism function in DN thymocytes, stringent regulation of *Tcrb* recombination would predict uniformly monoallelic *Tcrb* 53BP1 foci in Artemis-deficient thymocytes, because these thymocytes cannot repair RAG-induced coding ends and would signal continuously to suppress *Tcrb* recombination on the other allele. However, we found that nearly 10% of Artemis-deficient DN thymocyte nuclei contained two 53BP1^{+} *Tcrb* alleles. Moreover, if such a mechanism were active, it also should prevent concurrent rearrangement events at different TCR loci in DN thymocytes. However, nuclei with 53BP1 foci at two or three TCR loci do not appear to be underrepresented in WT DN thymocytes (22). We conclude that signaling downstream of an unrepaired *Tcrb* DSB is insufficient to ensure monoallelic RAG activity, perhaps because RAG protein expression cannot be downregulated rapidly enough to guarantee this outcome. It remains unclear whether this insufficiency applies selectively to D_β-to-J_β recombination, which likely predominates in Artemis-deficient DN thymocyte nuclei, or applies to V_β-to-DJ_β recombination as well.

Our conformational analysis of the *Tcrb* locus suggested that on most lamin-associated *Tcrb* alleles both the V_β and C_β ends of the locus were associated with the nuclear lamina. However, on 53BP1^{+} *Tcrb* alleles, the 53BP1 focus generally was farther from the nuclear lamina than the lamin-associated V_β and C_β end of the locus. Our interpretation was that one end of the locus had dissociated from the lamina and therefore was permissive for recombination. However, an alternate interpretation of our results would be that 53BP1^{+} *Tcrb* alleles are anchored to the lamina via both ends of the locus, with 53BP1 accumulating on central *Tcrb*-locus DNA that loops away from the periphery. We could not analyze this possibility directly, because technical limitations prevented us from performing four-color 3D immuno-FISH analysis in which the nuclear lamina, 53BP1, the V_β end, and the C_β end of the *Tcrb* locus could be labeled

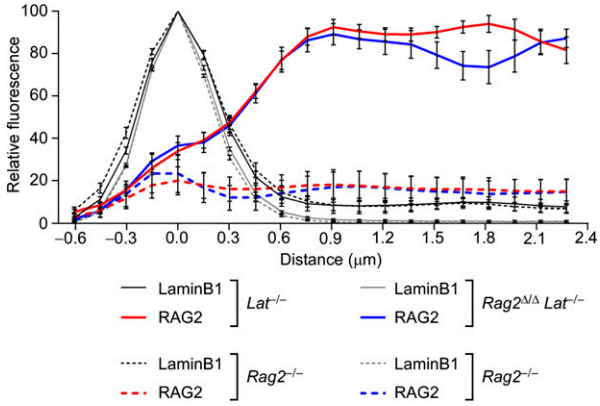

Fig. 7. The RAG2 PHD domain is not required for RAG2 localization to the nuclear interior. Normalized distributions of RAG2 and laminB1 fluorescence intensity across *Lat*$^{-/-}$, *Rag2*$^{\Delta/\Delta}$, and *Rag2*$^{-/-}$ DN thymocyte nuclei. The RAG2 (red) and laminB1 (black) fluorescence intensity plots for *Lat*$^{-/-}$ and its corresponding *Rag2*$^{-/-}$ staining are from Fig. 4*D*. Slides containing *Rag2*$^{\Delta/\Delta}$ *Lat*$^{-/-}$ nuclei were stained and imaged together with an additional set of slides containing *Rag2*$^{-/-}$ nuclei to allow evaluation of relative fluorescence intensities (RAG2, blue; laminB1, gray). Traces were aligned and normalized as in Fig. 4*D*. Data were collected for 40 nuclear edges per experiment. Each trace represents the mean ± SEM of four or five independent experiments.

simultaneously and distinctly. However, our observation that D_β-to-J_β recombination is inhibited on alleles anchored to the lamina via their C_β but not their V_β end argues, at a minimum, that these must represent two conformationally distinct subsets of alleles.

An important unresolved question is the mechanism by which the *Tcrb* locus is positioned at the nuclear lamina. A recent publication identified specific DNA sequences in the lamin-associated *Igh* and *Cyp3a* genes that could recruit heterologous genes to the lamina in NIH 3T3 cells (36). These fragments contain multiple binding motifs for the transcriptional repressor cKrox. Additionally, both cKrox and its interaction partner HDAC3 were shown to be significant mediators of *Igh* and *Cyp3a* lamin association. CTCF also has been implicated in perinuclear positioning of a subtelomeric element (59) and of the inactive human cystic fibrosis transmembrane conductance regulator gene (60). More recently, high AT content was shown to be a defining feature of constitutive LADs (61). It will be important to dissect the *Tcrb* locus with the goal of identifying peripheral targeting elements and transacting factors in future experiments.

Although we found that the majority of *Tcrb* alleles are present at the nuclear periphery in an environment characterized by reduced levels of RAG2, ChIP analysis has demonstrated abundant RAG2 binding to D_β and J_β segments in DN thymocytes (47). Although these results seem contradictory, it is important to consider that ChIP provides only a population analysis that cannot discriminate heterogeneity of RAG2 binding on different alleles. We suggest that the RAG2 ChIP signals reflect RAG2 binding on the subset of *Tcrb* alleles that are free of the nuclear lamina and the subset of peripheral *Tcrb* alleles whose D_β and J_β segments are dissociated from the lamina.

Although we have documented reduced RAG2 levels at the nuclear periphery, we cannot formally rule out the possibility that the nuclear periphery also may inhibit *Tcrb* recombination by other mechanisms. For example, the nuclear periphery could exclude other components of the V(D)J recombination machinery, including RAG1 and DSB repair factors. Moreover, because the nuclear periphery is generally suppressive for gene expression, it remains possible that the nuclear periphery suppresses *Tcrb* recombination by regulating locus transcription and accessibility. One argument against this possibility was a study in which a knockin reporter of Vβ8.2 expression was shown to be biallelically transcribed in all DN thymocytes (12). However, the possibility that Vβ8.2 has atypical expression characteristics or that its expression was perturbed by introduction of the reporter could not be formally excluded. Consistent with the notion of biallelic transcription irrespective of subnuclear localization, we detected PolII at 80–90% of lamin-associated and free *Tcrb* alleles in DN thymocyte nuclei. However, colocalization with PolII does not indicate transcription. Thus, in future studies it will be important to evaluate by RNA-FISH whether germ-line transcription is equivalent on lamin-associated and free *Tcrb* alleles.

The molecular basis for the RAG2 distribution in DN thymocyte nuclei remains unknown. RAG2 is known to interact with the active histone modification H3K4me3 (40, 41), and ChIP-sequencing analysis has revealed very high concordance between RAG2 binding and H3K4me3 islands genome wide (47). Although we could not compare the subnuclear distributions of RAG2 and H3K4me3 directly, our data do argue that the overall RAG2 distribution is not defined by that of H3K4me3. This apparent discrepancy may reflect the fact that the population view afforded by ChIP-sequencing overlooks the dynamic nature of the spatial relationship between RAG2 and transcription factories. We suggest that DN thymocyte nuclei may contain both chromatin-bound and -free pools of RAG2. We further suggest that RAG2 may move in and out of transcription factories [which themselves appear to be quite dynamic (62)], interacting with only a subset of actively transcribed genes at any moment in individual nuclei. Consistent with the idea that most nuclear RAG2 is either weakly associated or unassociated with chromatin, RAG2 (but not PolII) staining was greatly diminished when cells were briefly incubated with a standard Triton X-100 wash buffer before fixation (Fig. S2). We contend that the subnuclear distribution of this pool of RAG2 is highly

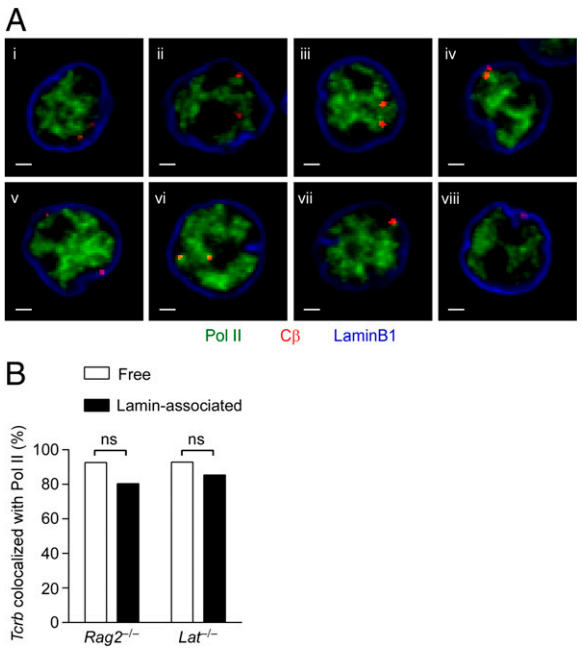

Fig. 8. Nearly all *Tcrb* alleles colocalize with PolII. (*A*) Confocal immuno-FISH microscopy showing the relative locations of *Tcrb*, PolII, and laminB1 in single z-slice images of *Lat*$^{-/-}$ DN thymocyte nuclei. *Tcrb* alleles were identified by hybridization with the C_β-end probe. (Scale bars, 1 μm.) (*B*) Frequencies of lamin-associated and free *Tcrb* alleles that colocalize with PolII. Data were collected from 160 alleles in *Rag2*$^{-/-}$ and 186 alleles in *Lat*$^{-/-}$ DN thymocytes; ns, not significant using Fisher's exact two-tailed contingency tables.

relevant for the regulation of V(D)J recombination, because this pool would serve as the local source of RAG2 that becomes functionally associated with antigen-receptor loci. Additional studies clearly will be required to provide greater understanding of the assembly, subnuclear dynamics, and functional characteristics of recombinase foci in nuclei of developing lymphocytes.

Materials and Methods

Mice. *Rag2*$^{-/-}$ (63), *Lat*$^{-/-}$ (21), ω (37), M4 (37), DJβ (38), Artemis$^{-/-}$ (64), *Rag2*$^{\Delta/\Delta}$ (48), and μMT (65) mice were described previously. All mice were used in accordance with protocols approved by the Duke University Animal Care and Use Committee.

Cell Collection. DN thymocytes were obtained directly from 2- to 3-wk-old mice as previously described (14). DP and CD4^{+}CD8^{-} thymocytes were sorted from 2- to 3-wk-old C57BL/6 or 129 mice using FITC-conjugated anti-CD4 (GK1.5) and Pacific Blue-conjugated anti-CD8α (53–6.7). Mature splenic B cells were obtained by sorting using Fc-block, anti-CD19 BIO (6D5) plus FITC-conjugated streptavidin, and Pacific Blue-conjugated anti-B220 (RA3-6B2). Pro-B cells were sorted from 4- to 6-wk-old μMT mice using FITC-conjugated anti-CD43 (S11) and Pacific Blue-conjugated anti-B220 (RA3-6B2). All antibodies were obtained from BioLegend.

FISH Probes and Antibodies. BAC clones RP23-75P5 (at the V_{β} end of the *Tcrb* locus) and RP23-457D7 (at the C_{β} end of the *Tcrb* locus) were used as DNA probes. BAC clones were labeled using either a digoxigenin or biotin nick-translation kit (Roche). Foci were visualized with either FITC-conjugated anti-biotin (200-092-211; Jackson ImmunoResearch Laboratories) or Cy3-conjugated anti-digoxigenin (200-162-156; Jackson ImmunoResearch Laboratories). The nuclear lamina was visualized using a polyclonal goat anti-laminB1 antibody (sc-6217; Santa Cruz Biotechnology) and Cy5-conjugated anti-goat antibodies (705-605-003; Jackson ImmunoResearch Laboratories). 53BP1 was visualized using a polyclonal rabbit anti-53BP1 antibody (NB 100–304; Novus Biologicals) and FITC-conjugated donkey anti-rabbit IgG (sc-2090; Santa Cruz Biotechnology). Ki67 was visualized using a polyclonal mouse anti-Ki67 antibody (556003; BD Pharmingen) and FITC-conjugated donkey anti-mouse IgG (715-095-150; Jackson ImmunoResearch Laboratories). RAG2 was visualized using monoclonal rabbit anti-RAG2 antibody no. 39 (43) and Cy3-conjugated goat anti-rabbit IgG F(ab′)$_2$ antibody (111-166-047; Jackson ImmunoResearch Laboratories). PolII was visualized using a monoclonal mouse anti-PolII antibody (NB200-598; Novus Biologicals) and FITC-conjugated donkey anti-mouse IgG (715-545-151; Jackson ImmunoResearch Laboratories). H3K4me3 was visualized using a polyclonal rabbit anti-H3K4me3 antibody (ab8580; Abcam) and either Cy3-conjugated donkey anti-rabbit IgG (711-165-152; Jackson ImmunoResearch Laboratories) or FITC-conjugated donkey anti-rabbit IgG (711-095-152; Jackson ImmunoResearch Laboratories).

3D DNA Immuno-FISH and Confocal Imaging. Methods for cell fixation and immuno-FISH were as described (14) except that slides were denatured at 77.8 °C before hybridization and were washed twice in 50% (vol/vol) formamide at 40 °C and three times in 0.2× SSC at 60 °C. Each slide received 0.5–1 μg of primary antibody and 3–5 μg of conjugated secondary antibody in 0.4 mL of 4% (wt/vol) BSA and 2× SSC. The specificity of PolII and H3K4me3 staining was demonstrated by preincubation of primary antibody for each slide with 8 μg of PolII (ab18488; Abcam) and H3K4me3 (ab1342; Abcam) peptide-immunogen, respectively, for 30 min at 23 °C before staining of nuclei. Slides were imaged on a Leica SP5 confocal microscope. Optical sections separated by 0.12 μm were collected, and only cells with intact laminB1 signals were analyzed. Nucleoplasmic proteins were extracted from cells by incubation of slides as previously described (66), except that cells were treated with 0.5% (vol/vol) Triton X-100, 20 mM Hepes (pH 7.9), 3 mM $MgCl_2$, and 300 mM sucrose containing 0–100 mM NaCl for only 1 min. Slides then were processed for 3D immunofluorescence as described above.

Colocalization Analysis. All colocalization experiments were performed using ImageJ software. Images initially were passed through a Kalman stack filter and then were thresholded so that (*i*) the laminB1 signal formed a contiguous ring around most nuclei, (*ii*) two BAC probe signals were present within most nuclei, and (*iii*) low-level 53BP1, RAG2, Pol II, H3K4me3, and DAPI signals were eliminated. Background RAG2 staining (as judged by the signal in *Rag2*$^{-/-}$ nuclei) was higher in immuno-FISH than in simple immunofluorescence experiments. The 3D distance between the centers of mass of two foci was measured using the Sync Measure 3D ImageJ plugin. Foci were considered colocalized with laminB1, RAG2, or PolII if two adjacent pixels overlapped.

Conformation Analysis. To determine the orientation of peripheral *Tcrb* alleles, images were deconvolved using Huygens Essential software with specifications appropriate for a Leica SP5 confocal microscope with a 100× objective and 2× zoom. Distance from the nuclear lamina was determined by measuring from the center of mass of each focus to the nearest point on the inner edge of the nuclear lamina. Foci whose volume was >50% colocalized with the nuclear lamina were considered to have a center of mass internal to the lamina and were assigned a positive distance value. Foci whose volume was <50% colocalized with the lamina were considered to have a center of mass external to the lamina and were assigned a negative distance value. To determine the peripheral location of the experimental focus in relation to the lamin-anchored focus, the distance of the experimental focus was subtracted from the distance of the lamin-anchored focus.

Fluorescence Intensity Traces. Fluorescence intensity plots were obtained using the Twin Slicer application of Huygens Essential deconvolution software. One z-slice within the middle third of each nucleus was selected for analysis, and fluorescence intensity was traced along a single diameter within this z-slice. Gene location relative to the nuclear periphery was determined by selecting a z-slice in the middle third of the nucleus in which the allele focus was brightest. Lines then were traced through the brightest portion of the focus to the nearest point on the nuclear lamina.

Correlation Analysis. Correlation analysis was conducted on raw image stacks. Pearson's correlation coefficient, *r*, was calculated as a measure of the average colocalization between two markers within cells. To restrict the analysis to cells which had been properly labeled, as well as to get an idea of inter-cell variability, we calculated *r* for individual cells that were selected based on nuclear structure and the presence of each marker. To this end, individual nuclei in the field of view were segmented from 3D image stacks using laminB1 to mark nuclear boundaries. All nuclear boundaries in the field of view were identified using a fixed threshold of laminB1 signal. The resulting binary image was segmented into individual nuclei using a connected components identification algorithm (67) combined with morphological closing (68). Correlation was calculated in the interior of each identified nucleus. Image processing was carried out in MATLAB.

To compare colocalization in PolII vs. H3K4me3 against the colocalization in PolII vs.RAG2, we fit a model of the form:

$$r_{ij} = \mu^{H} + \mu_i^{R-H} + f_i + \varepsilon_{ij}$$

where r_{ij} is the Pearson's correlation (whole-cell colocalization) for the *j*-th cell in the *i*-th field of view ($i = 1, \ldots, 10$). The baseline mean (for PolII vs. H3K4me3) is denoted by μ^{H}. For fields of view *i* in the PolII vs.RAG2 experiments, the term μ_i^{R-H} denotes the difference of the mean colocalization between PolII vs.RAG2 compared with the colocalization between mPolII vs. H3K4me3. The term f_i is an effect which captures the variability caused by the *i*-th field of view. It is assumed to be random and to have a Gaussian distribution with 0 mean and constant SD σ. Finally ε_{ij} denotes measurement error. The model is fitted using restricted maximum likelihood using the nlme package in the R computing platform.

ACKNOWLEDGMENTS. We thank S. Johnson and Y. Gao of the Duke Comprehensive Cancer Center Light Microscopy Facility for imaging support, F. W. Alt for providing DJβ/DJβ mice, and B. Jones-Mason and H.-Y. Shih for helpful comments on the manuscript. This work was supported by National Institutes of Health Grants R01 AI49934 (to M.S.K.), R37 AI32524 (to D.G.S.), and R01 CA12595 (to C.H.B.).

1. Schatz DG, Swanson PC (2011) V(D)J recombination: Mechanisms of initiation. *Annu Rev Genet* 45:167–202.
2. Schatz DG, Ji Y (2011) Recombination centres and the orchestration of V(D)J recombination. *Nat Rev Immunol* 11(4):251–263.
3. Brady BL, Steinel NC, Bassing CH (2010) Antigen receptor allelic exclusion: An update and reappraisal. *J Immunol* 185(7):3801–3808.
4. Vettermann C, Schlissel MS (2010) Allelic exclusion of immunoglobulin genes: Models and mechanisms. *Immunol Rev* 237(1):22–42.
5. Krangel MS (2009) Mechanics of T cell receptor gene rearrangement. *Curr Opin Immunol* 21(2):133–139.
6. Michie AM, Zúñiga-Pflücker JC (2002) Regulation of thymocyte differentiation: Pre-TCR signals and β-selection. *Semin Immunol* 14(5):311–323.

7. Tripathi R, Jackson A, Krangel MS (2002) A change in the structure of Vbeta chromatin associated with TCR β allelic exclusion. *J Immunol* 168(5):2316–2324.
8. Skok JA, et al. (2007) Reversible contraction by looping of the *Tcra* and *Tcrb* loci in rearranging thymocytes. *Nat Immunol* 8(4):378–387.
9. Jackson A, Kondilis HD, Khor B, Sleckman BP, Krangel MS (2005) Regulation of T cell receptor β allelic exclusion at a level beyond accessibility. *Nat Immunol* 6(2):189–197.
10. Kondilis-Mangum HD, Shih HY, Mahowald G, Sleckman BP, Krangel MS (2011) Regulation of TCRβ allelic exclusion by gene segment proximity and accessibility. *J Immunol* 187(12):6374–6381.
11. Ranganath S, et al. (2008) Productive coupling of accessible Vbeta14 segments and DJbeta complexes determines the frequency of Vbeta14 rearrangement. *J Immunol* 180(4):2339–2346.
12. Jia J, Kondo M, Zhuang Y (2007) Germline transcription from T-cell receptor Vbeta gene is uncoupled from allelic exclusion. *EMBO J* 26(9):2387–2399.
13. Roldán E, et al. (2005) Locus 'decontraction' and centromeric recruitment contribute to allelic exclusion of the immunoglobulin heavy-chain gene. *Nat Immunol* 6(1): 31–41.
14. Schlimgen RJ, Reddy KL, Singh H, Krangel MS (2008) Initiation of allelic exclusion by stochastic interaction of *Tcrb* alleles with repressive nuclear compartments. *Nat Immunol* 9(7):802–809.
15. Kosak ST, et al. (2002) Subnuclear compartmentalization of immunoglobulin loci during lymphocyte development. *Science* 296(5565):158–162.
16. Noon AT, Goodarzi AA (2011) 53BP1-mediated DNA double strand break repair: Insert bad pun here. *DNA Repair (Amst)* 10(10):1071–1076.
17. Asaithamby A, Chen DJ (2009) Cellular responses to DNA double-strand breaks after low-dose γ-irradiation. *Nucleic Acids Res* 37(12):3912–3923.
18. Difilippantonio S, et al. (2008) 53BP1 facilitates long-range DNA end-joining during V(D)J recombination. *Nature* 456(7221):529–533.
19. Liu X, et al. (2012) Overlapping functions between XLF repair protein and 53BP1 DNA damage response factor in end joining and lymphocyte development. *Proc Natl Acad Sci USA* 109(10):3903–3908.
20. Bothmer A, et al. (2011) Regulation of DNA end joining, resection, and immunoglobulin class switch recombination by 53BP1. *Mol Cell* 42(3):319–329.
21. Zhang W, Sloan-Lancaster J, Kitchen J, Trible RP, Samelson LE (1998) LAT: The ZAP-70 tyrosine kinase substrate that links T cell receptor to cellular activation. *Cell* 92(1): 83–92.
22. Bowen S, Wangsa D, Ried T, Livak F, Hodes RJ (2013) Concurrent V(D)J recombination and DNA end instability increase interchromosomal trans-rearrangements in ATM-deficient thymocytes. *Nucleic Acids Res* 41(8):4535–4548.
23. Anderson L, Henderson C, Adachi Y (2001) Phosphorylation and rapid relocalization of 53BP1 to nuclear foci upon DNA damage. *Mol Cell Biol* 21(5):1719–1729.
24. Gerace L, Huber MD (2012) Nuclear lamina at the crossroads of the cytoplasm and nucleus. *J Struct Biol* 177(1):24–31.
25. Kind J, van Steensel B (2010) Genome-nuclear lamina interactions and gene regulation. *Curr Opin Cell Biol* 22(3):320–325.
26. Pickersgill H, et al. (2006) Characterization of the *Drosophila melanogaster* genome at the nuclear lamina. *Nat Genet* 38(9):1005–1014.
27. Guelen L, et al. (2008) Domain organization of human chromosomes revealed by mapping of nuclear lamina interactions. *Nature* 453(7197):948–951.
28. Peric-Hupkes D, et al. (2010) Molecular maps of the reorganization of genome-nuclear lamina interactions during differentiation. *Mol Cell* 38(4):603–613.
29. Hewitt SL, High FA, Reiner SL, Fisher AG, Merkenschlager M (2004) Nuclear repositioning marks the selective exclusion of lineage-inappropriate transcription factor loci during T helper cell differentiation. *Eur J Immunol* 34(12):3604–3613.
30. Zink D, et al. (2004) Transcription-dependent spatial arrangements of CFTR and adjacent genes in human cell nuclei. *J Cell Biol* 166(6):815–825.
31. Williams RR, et al. (2006) Neural induction promotes large-scale chromatin reorganisation of the Mash1 locus. *J Cell Sci* 119(Pt 1):132–140.
32. Peric-Hupkes D, van Steensel B (2010) Role of the nuclear lamina in genome organization and gene expression. *Cold Spring Harb Symp Quant Biol* 75:517–524.
33. Finlan LE, et al. (2008) Recruitment to the nuclear periphery can alter expression of genes in human cells. *PLoS Genet* 4(3):e1000039.
34. Kumaran RI, Spector DL (2008) A genetic locus targeted to the nuclear periphery in living cells maintains its transcriptional competence. *J Cell Biol* 180(1):51–65.
35. Reddy KL, Zullo JM, Bertolino E, Singh H (2008) Transcriptional repression mediated by repositioning of genes to the nuclear lamina. *Nature* 452(7184):243–247.
36. Zullo JM, et al. (2012) DNA sequence-dependent compartmentalization and silencing of chromatin at the nuclear lamina. *Cell* 149(7):1474–1487.
37. Bassing CH, et al. (2000) Recombination signal sequences restrict chromosomal V(D)J recombination beyond the 12/23 rule. *Nature* 405(6786):583–586.
38. Carpenter AC, et al. (2009) Assembled DJ β complexes influence TCR β chain selection and peripheral V β repertoire. *J Immunol* 182(9):5586–5595.
39. Yao J, Fetter RD, Hu P, Betzig E, Tjian R (2011) Subnuclear segregation of genes and core promoter factors in myogenesis. *Genes Dev* 25(6):569–580.
40. Liu Y, Subrahmanyam R, Chakraborty T, Sen R, Desiderio S (2007) A plant homeodomain in RAG-2 that binds Hypermethylated lysine 4 of histone H3 is necessary for efficient antigen-receptor-gene rearrangement. *Immunity* 27(4):561–571.
41. Matthews AG, et al. (2007) RAG2 PHD finger couples histone H3 lysine 4 trimethylation with V(D)J recombination. *Nature* 450(7172):1106–1110.
42. Elkin SK, et al. (2005) A PHD finger motif in the C terminus of RAG2 modulates recombination activity. *J Biol Chem* 280(31):28701–28710.
43. Coster G, Gold A, Chen D, Schatz DG, Goldberg M (2012) A dual interaction between the DNA damage response protein MDC1 and the RAG1 subunit of the V(D)J recombinase. *J Biol Chem* 287(43):36488–36498.
44. Kubbutat MH, et al. (1994) Epitope analysis of antibodies recognising the cell proliferation associated nuclear antigen previously defined by the antibody Ki-67 (Ki-67 protein). *J Clin Pathol* 47(6):524–528.
45. Li Z, Dordai DI, Lee J, Desiderio S (1996) A conserved degradation signal regulates RAG-2 accumulation during cell division and links V(D)J recombination to the cell cycle. *Immunity* 5(6):575–589.
46. Vermeulen M, et al. (2010) Quantitative interaction proteomics and genome-wide profiling of epigenetic histone marks and their readers. *Cell* 142(6):967–980.
47. Ji Y, et al. (2010) The *in vivo* pattern of binding of RAG1 and RAG2 to antigen receptor loci. *Cell* 141(3):419–431.
48. Liang HE, et al. (2002) The "dispensable" portion of RAG2 is necessary for efficient V-to-DJ rearrangement during B and T cell development. *Immunity* 17(5):639–651.
49. Lisby M, Mortensen UH, Rothstein R (2003) Colocalization of multiple DNA double-strand breaks at a single Rad52 repair centre. *Nat Cell Biol* 5(6):572–577.
50. Aten JA, et al. (2004) Dynamics of DNA double-strand breaks revealed by clustering of damaged chromosome domains. *Science* 303(5654):92–95.
51. Nelms BE, Maser RS, MacKay JF, Lagally MG, Petrini JH (1998) *In situ* visualization of DNA double-strand break repair in human fibroblasts. *Science* 280(5363):590–592.
52. Kruhlak MJ, et al. (2006) Changes in chromatin structure and mobility in living cells at sites of DNA double-strand breaks. *J Cell Biol* 172(6):823–834.
53. Soutoglou E, et al. (2007) Positional stability of single double-strand breaks in mammalian cells. *Nat Cell Biol* 9(6):675–682.
54. Roukos V, et al. (2013) Spatial dynamics of chromosome translocations in living cells. *Science* 341(6146):660–664.
55. Hakim O, et al. (2012) DNA damage defines sites of recurrent chromosomal translocations in B lymphocytes. *Nature* 484(7392):69–74.
56. Zhang Y, et al. (2012) Spatial organization of the mouse genome and its role in recurrent chromosomal translocations. *Cell* 148(5):908–921.
57. Bednarski JJ, Sleckman BP (2012) Integrated signaling in developing lymphocytes: The role of DNA damage responses. *Cell Cycle* 11(22):4129–4134.
58. Steinel NC, et al. (2013) The ataxia telangiectasia mutated kinase controls Igκ allelic exclusion by inhibiting secondary Vκ-to-Jκ rearrangements. *J Exp Med* 210(2): 233–239.
59. Ottaviani A, et al. (2009) Identification of a perinuclear positioning element in human subtelomeres that requires A-type lamins and CTCF. *EMBO J* 28(16):2428–2436.
60. Muck JS, Kandasamy K, Englmann A, Günther M, Zink D (2012) Perinuclear positioning of the inactive human cystic fibrosis gene depends on CTCF, A-type lamins and an active histone deacetylase. *J Cell Biochem* 113(8):2607–2621.
61. Meuleman W, et al. (2013) Constitutive nuclear lamina-genome interactions are highly conserved and associated with A/T-rich sequence. *Genome Res* 23(2):270–280.
62. Cisse II, et al. (2013) Real-time dynamics of RNA polymerase II clustering in live human cells. *Science* 341(6146):664–667.
63. Shinkai Y, et al. (1992) RAG-2-deficient mice lack mature lymphocytes owing to inability to initiate V(D)J rearrangement. *Cell* 68(5):855–867.
64. Rooney S, et al. (2002) Leaky Scid phenotype associated with defective V(D)J coding end processing in Artemis-deficient mice. *Mol Cell* 10(6):1379–1390.
65. Kitamura D, Roes J, Kühn R, Rajewsky K (1991) A B cell-deficient mouse by targeted disruption of the membrane exon of the immunoglobulin μ chain gene. *Nature* 350 (6317):423–426.
66. Li B, de Lange T (2003) Rap1 affects the length and heterogeneity of human telomeres. *Mol Biol Cell* 14(12):5060–5068.
67. Haralick RM, Shapiro LG (1992) *Computer and robot vision* (Addison-Wesley Pub. Co, Reading, Mass).
68. Soille P (2003) *Morphological Image Analysis: Principles and Applications* (Springer, Secaucus, NJ), 2nd Ed.